J Mater Sci (2016) 51:6933–6943

Tailoring the mechanical properties of thermoelectric lead telluride by alloying with non-doping calcium

Andreas Schmitz[1,*], Johannes de Boor[1], Klaus Mull[1], and Eckhard Müller[1,2]

[1] *Institute of Materials Research, German Aerospace Center (DLR), Linder Hoehe, 51147 Cologne, Germany*
[2] *Institute for Inorganic and Analytical Chemistry, Justus-Liebig-University, Heinrich-Buff-Ring 58, 35392 Giessen, Germany*

Received: 11 February 2016
Accepted: 11 April 2016
Published online: 20 April 2016

ABSTRACT

Thermoelectric generators have a great potential in waste heat recovery and energy harvesting due to their principle of directly converting thermal into electrical energy. Despite a long history in space travel and a broad range of potential applications, TEGs are rarely found in terrestrial applications. Reasons are manufacturing problems and limited durability in dynamic operation conditions due to deficient mechanical properties of the thermoelectric materials, which often suffer from low strength and high brittleness. We present a concept for the basically independent tailoring of mechanical and thermoelectric properties. This can be achieved by the alloying of TE materials with additional elements having preferably no or only little influence on the TE properties. We demonstrate a route of improving the mechanical properties of PbTe by alloying with calcium. It is shown that calcium has minor effects on the thermoelectric properties of PbTe while significantly increasing hardness and fracture strength. As proof of concept, mechanically more stable sodium and calcium co-doped $Pb_{0.966}Ca_{0.02}Na_{0.014}Te$ with ZT exceeding 1.2 above 650 K is demonstrated.

Introduction

Thermoelectric generators (TEG) have attracted great attention in recent years due to their potential in energy harvesting and waste heat recovery applications providing direct conversion of thermal into electrical energy. The durability of TEGs in terrestrial applications such as automotive exhaust waste heat recovery is still a major issue, whereas in space mission applications thermoelectric generators have proven their reliability over decades of operation [1–5]. Durability issues are partly due to mechanical and thermomechanical stresses arising from external mechanical loads like vibrations as well as fast changing thermal conditions on the hot and cold side and mismatches in the coefficients of thermal expansion [5, 6]. Besides failure of the contact between thermoelectric material and metal bridge a fracture of the thermoelectric leg itself is a major concern. Being highly doped semiconductors, thermoelectric materials are often very brittle and may show low fracture strengths. As a consequence, there have been some attempts in recent years to improve

Address correspondence to E-mail: a.schmitz@dlr.de

DOI 10.1007/s10853-016-9980-x

these mechanical properties in different classes of thermoelectric materials [7–10].

Lead telluride (PbTe) has been used as thermoelectric material in an intermediate temperature range up to 450 °C for decades [2, 3, 11, 12]. Its advantages are the good availability of p- and n-type material and thermoelectric figures of merit *ZT* around 2.0 which is among the highest of all know thermoelectric materials [13–19]. Still the mechanical properties of PbTe are a major drawback: PbTe has a very high coefficient of thermal expansion around 2×10^{-5} K^{-1} [5, 20, 21], increasing the issue of thermal expansion-related stresses. Furthermore, lead telluride is rather soft and brittle with low fracture strength compared to for example skutterudites [22–28]. This is particularly true for p-type lead telluride as at a charge carrier concentration around 3×10^{19} cm^{-3} the brittleness increases even further [23].

In this context, an improvement of the mechanical properties of thermoelectric materials is of great importance for their potential use in a broad range of applications. In this study, lead telluride is chosen as a model system due to its good thermoelectric properties, availability, and rather simple structure.

Earlier attempts to improve the mechanical properties of PbTe relied on introducing inert particles or fibres into the PbTe matrix to form a composite material. Especially molybdenum, tungsten or Al_2O_3 were used, leading to increased fracture toughness [29]. Furthermore, composites of PbTe were produced by mixing with PbS or PbSe or by adding silicon [30, 31]. In all the cases, increased hardness values were obtained and attributed to the formation of nano and micro composites with precipitations of the added components.

In this work, the idea is to improve the mechanical properties of lead telluride by alloying instead of using microstructural effects. It is well known that alloying or doping PbTe with other elements may have a strong influence on its mechanical properties [23, 25–27, 32]. While these influences on the mechanical properties have so far been an inevitable side effect of doping for optimal thermoelectric properties, the approach in this study is different. The idea is to alloy PbTe with additional, virtually non-doping elements with the goal of purposefully changing the mechanical properties while trying to keep the thermoelectric properties unchanged as far as possible. Within this work, the described concept is being tested on undoped stoichiometric PbTe. Calcium is chosen as element for altering the mechanical properties. Calcium is a good candidate as it is bivalent just as lead to substitute the latter within the PbTe lattice. Furthermore, calcium is completely mixable with PbTe above 200 K [33]. Additionally, a sample of sodium-doped p-type PbTe is co-doped with calcium as first proof of concept in doped material.

Material preparation and measurements

Pre-alloyed PbTe of purity 5 N was sealed in evacuated quartz ampoules together with elemental calcium and/or sodium with stoichiometry $Pb_{1-(x+y)}Ca_xNa_yTe$. The ampoules were then heated to 1323 K in a rocking furnace. Two different routes were chosen for the further treatment: First (batch 1), ampoules were kept at this temperature for 10 h and cooled down slowly within 48 h to 973 K and then down to room temperature in another 12 h, similar to the route described by Ahn et al. [34].

The alternative second route utilizes water-quenching after 2 h of rocking at 1323 K. In this route, the ingots are subsequently annealed at 973 K for 140 h to ensure phase homogeneity (batch 2 and 3).

The material was ground by hand to obtain powders with average particle sizes of 120 μm (batch 1) and 60 μm (batch 2 and 3), measured with a Beckman Coulter LS 13320 particle analyser. Bulk samples of 12.7 mm in diameter and about 2 mm in thickness were sintered at 673–723 °C and 40 MPa in a short-term sintering process. This sintering technique is similar to common spark plasma sintering (SPS) except for the use of continuous instead of pulsed DC heating current. All sintered samples within this work have densities above 98 % of the theoretical density. For the calcium containing samples, the theoretical density was calculated as a linear interpolation between pure PbTe and CaTe.

The phase composition of the powders was investigated prior to sintering using a Siemens Bruker D5000 powder diffractometer. To determine the lattice constant, LaB_6 was mixed into the powder as reference material. Recorded data was analysed by Rietveld refinement using the FullProf software [35, 36]. Additionally SEM with EDX was used to analyse the sintered samples' microstructure. Sample

homogeneity was checked employing the Potential & Seebeck Microprobe (PSM), with which the spatial distribution of the Seebeck coefficient on ingots as well as on sintered samples was measured [37].

The thermal diffusivity was measured with a Netzsch LFA 427. For calculation of the thermal conductivity, the theoretical heat capacity $c_p = 0.149$ J/(g K) calculated according to Dulong–Petit's law was used as the temperatures investigated here are far above the Debye temperature of PbTe [21, 38]. This theoretical value matches very well with experimental c_p data by other authors [12, 39].

Temperature-dependent Seebeck coefficient and electrical conductivity were measured concurrently using a custom-built facility [40]. In both measurements—LFA and Seebeck/sigma—the samples' properties were measured during the heating and cooling cycle to obtain information on the thermal stability of the material. Experimental errors are assumed to be 10, 5 and 7 % for thermal conductivity, electrical conductivity and Seebeck coefficient, respectively [41].

For the mechanical characterization, hardness measurements as well as uniaxial compression tests were performed at room temperature. The hardness measurements were done using a Vickers indenter and an indentation force of 0.49 N. Results were averaged over in total 100 indentations on both sides of the sintered pellets. Error bars in the hardness figures indicate the standard deviation of the measured values. Compression tests were performed on two to three cubes of $4 \times 4 \times 4$ mm^3 for each composition and at a compression speed of 0.5 mm/min.

Results and discussion

Calcium in pure PbTe

To gain insight into the influence of calcium on PbTe, especially on how much it influences the electronic and thus thermoelectric properties, alloys of calcium and pure, undoped PbTe were synthesized so that effects of calcium are not superimposed by effects of other dopants. For batch 1, calcium concentrations of $x = 0.004$, 0.02, 0.04 and 0.06 were chosen. No secondary phases were detected in the XRD measurements in all samples after annealing. Furthermore the XRD measurements show no changes in the lattice constant (6.4604 ± 0.0008 Å) due to calcium. According to Vegard's law, a decrease of the lattice constant would be expected upon doping with calcium due to the smaller lattice constant of CaTe (6.358 Å) compared to PbTe (6.460 Å) [34]. As described by Biswas et al., the unchanged lattice constant might be an indication that only a fraction of the calcium is dissolved in the PbTe matrix while the rest forms precipitates of CaTe [42]. This might be a consequence of the chosen heat treatment during preparation or otherwise indicate that a solubility limit exists around $x = 0.02$ in contrast to the calculations by Sifi et al. [33].

To further investigate the microstructure of the sintered samples and possible precipitation SEM was employed. This revealed a broad distribution of grain sizes between 5 and 200 μm with small grains filling the voids between large ones. The grain size distribution corresponds well to the particle size distribution found in the powder indicating that the powder consisted mainly of single crystalline particles. No preferred orientation is visible in EBSD images. No CaTe precipitates could be detected by SEM although a large area of the sample surface was investigated at varying magnification. Thus the assumed CaTe precipitates might be too small in size to be observed in SEM.

PSM measurements reveal positive Seebeck coefficients at room temperature in all samples, indicating relative excess of tellurium within the matrix [43–45]. While no macroscopic gradient is visible in the PSM measurements, the measurements yield a broad distribution of Seebeck coefficient values with random local variations on a millimetre scale which is typical for such measurements of undoped PbTe (see Supplementary Fig. S1). SEM/EDX measurements confirmed tellurium excess in the matrix also revealing few, isolated, tellurium-rich precipitates within the PbTe matrix (see Supplementary Fig. S2).

Based on the results obtained with batch 1, a second batch of samples with $x = 0.002$, 0.004, 0.01, 0.02 and 0.03 (batch 2) was synthesized. An alternative heat treatment as described above was chosen to further reduce any precipitation. As the difference in material preparation between batches 1 and 2 may have an influence on the resulting functional properties, results of both batches are displayed in separate figures. A detailed analysis of the influence of heat treatment and powder particle size is beyond the scope of this work. Results of a detailed study on this topic will be published elsewhere. Calcium

concentrations in batch 2 were chosen to refine the concentration steps at lower concentrations as well as to allow a comparison between samples of the same composition but prepared by the two different routes.

As shown in Fig. 1 above roughly 600 K, the Seebeck coefficient S changes to negative values due dominance of intrinsic charge carriers at high temperatures, which is confirmed by the increasing electrical conductivity σ at high temperatures (see Fig. 2). In both batches, calcium addition leads to higher Seebeck values at low temperatures and lower absolute values in the intrinsic region at high temperatures. Furthermore calcium reduces the electrical conductivity especially in the low temperature regime, whereas its influence at high temperatures is much lower.

Both Seebeck coefficient and electrical conductivity suggest a reduction of the charge carrier concentration due to calcium at low temperatures. The Pisarenko relation can be employed to calculate the charge carrier concentration n based on the room temperature Seebeck values [34, 46–48]. Here acoustic phonon scattering is assumed and the hole effective mass is taken as 0.3 times the free electron mass [44]. Results of this calculation are shown in Fig. 3. An additional argument for the reduction of the room temperature charge carrier concentration due to calcium is the shift of the minimum of $\sigma(T)$ to lower temperatures (see esp. Fig. 2b). A comparison of n with the electrical conductivity $\sigma = en\mu$ furthermore indicates a reduction of the charge carrier mobility μ with increasing calcium content (Fig. 3b) in accordance with measurements in other publications [49, 50].

At high temperatures, Seebeck coefficient and electrical conductivity are dominated by intrinsic carriers. In this temperature region, the electrical conductivity σ can be written as

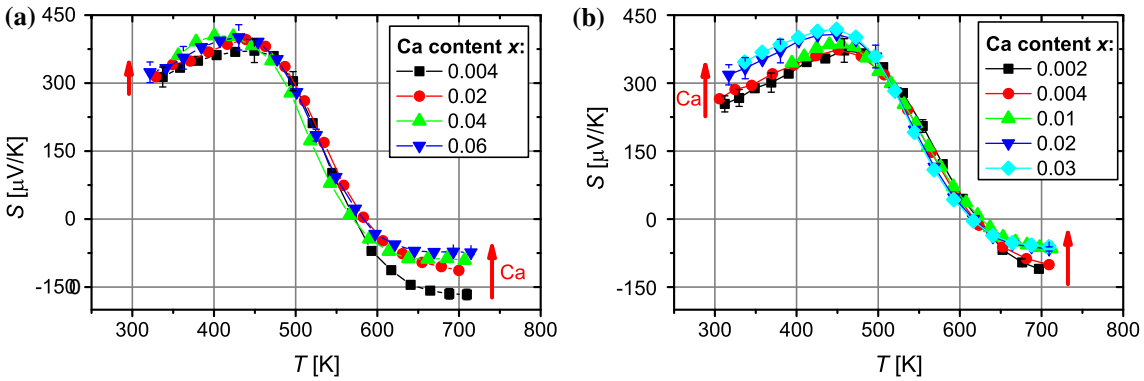

Figure 1 Temperature-dependent Seebeck coefficients of sintered samples of batch 1 (**a**) and 2 (**b**) with varying calcium content. Calcium leads to an increase of the Seebeck coefficient at low temperatures and a decrease at higher temperatures.

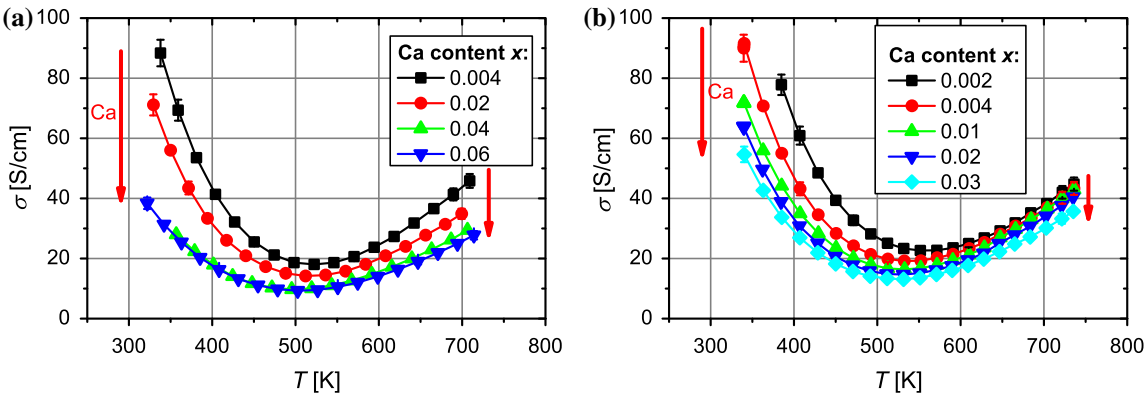

Figure 2 Temperature-dependent electrical conductivity of batch 1 (**a**) and 2 (**b**) samples with varying calcium content. An increasing calcium content leads to a reduction of the electrical conductivity which is most dominant at low temperatures. This also shifts the position of the electrical conductivity minimum to lower temperatures.

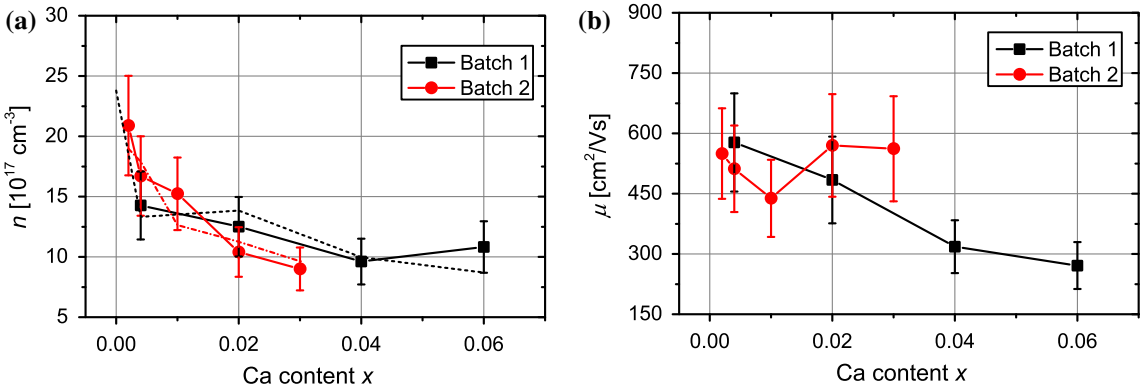

Figure 3 Charge carrier concentration (**a**) and mobility (**b**) at room temperature decrease with increasing calcium content. Values were calculated from Seebeck coefficient and electrical conductivity using Pisarenko's relation [26]. *Dashed lines* in (**a**) correspond to carrier concentrations calculated based on the band gap E_g.

$$\sigma = e\mu(T)c_N e^{-\frac{E_g}{2k_B T}} \quad (1)$$

with material specific constant c_N. Here $\mu(T)$ does not follow an exponential law. Thus the band gap E_g can be determined from the temperature dependence of the electrical conductivity as the slope of a linear fit of $\ln \sigma(T)$ over $1/T$ (see also Supplementary Fig. S3). As shown in Fig. 4, the band gap slightly increases from around 0.38 eV without calcium to 0.43 eV at calcium contents above $x = 0.03$. This is expected as CaTe has a bandgap ~4 eV and is attributed to the more ionic character of the Ca–Te binding compared to Pb–Te [34]. The band gap's increase follows Vegard's law only up to $x = 0.01$ and is less steep for higher calcium concentrations in both batches. This supports the assumption that at higher concentrations a part of the calcium forms CaTe precipitates [42].

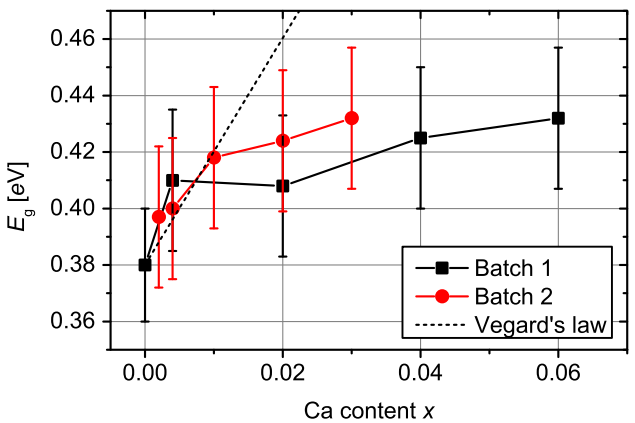

Figure 4 Electronic band gap of PbTe as a function of calcium content calculated from the electrical conductivity's temperature dependence in the intrinsic temperature range.

An increased band gap alone would shift the minimum of the electrical conductivity to higher temperatures which is in contrast to our observations shown in Fig. 2. We assume that the reduction in hole mobility and hole concentration at room temperature—which both shift the minimum of σ to lower temperatures—overcompensate the effect caused by the change of band gap.

To check whether the reduction of the room temperature carrier concentration shown in Fig. 3a) is a consequence of the increased band gap, carrier concentrations can be calculated based on the band gap values shown in Fig. 4 as

$$n = N_0 e^{-\frac{E_g}{2k_B T}} \quad (2)$$

with N_0 fitted to be 3.7×10^{21} and 4.1×10^{21} cm^{-3} for batches 1 and 2, respectively. These results—indicated as dashed lines in Fig. 3—resemble well the change of charge carrier concentration as function of calcium concentration and thus support the assumption that the reduction of the charge carrier concentration is caused by the increased band gap. The increased band gap and thus reduced carrier concentration leads to a reduction of the electrical conductivity. The fact that the values of N_0 are slightly different for both batches might be an indication of different defect state concentrations or tellurium content in both batches as a consequence of the different preparation routes.

The thermal conductivity of all batch 2 samples is slightly lower than that of batch 1 samples, which is attributed to microstructural differences as a result of the different preparation routes (Fig. 5): Slow cooling from the melt of batch 1 may have led to slightly

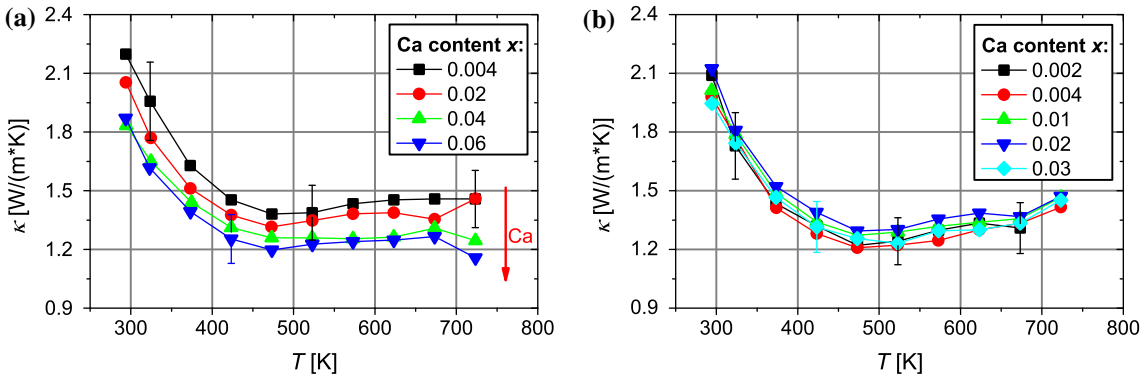

Figure 5 Temperature-dependent thermal conductivity of batch 1 (**a**) and 2 (**b**) sintered samples with varying calcium content.

larger grain sizes than quenching and annealing of batch 2. Additionally, the powder particle size of batch 2 is smaller than that of batch 1 by a factor of two.

The thermal conductivity is slightly reduced with increasing calcium content for the samples of batch 1, whereas no clear trend is visible in batch 2—probably due to smaller amounts of calcium and limitations given by measurement accuracy (see Fig. 5). The drop of thermal conductivity in batch 1 cannot solely be explained by the reduced electrical conductivity, as the total electronic contribution calculated by the Wiedemann–Franz law is lower than 0.1 W/(m·K) even at its maximum for all samples and temperatures investigated. As no difference in grain size and microstructure between the samples was observed, the reduction in lattice thermal conductivity at high calcium concentrations is due to increased phonon scattering. This could be caused lattice strain due to the calcium atoms and by the possible formation of nano-scale CaTe precipitates in accordance with our findings in lattice constant and electronic band gap [42]. Thus, at high calcium concentrations effects of precipitation act in addition to the effects caused by homogeneous alloying. Pure alloying effects were the primary goal of this study but obviously some precipitation could not be prevented.

Micro hardness measurements reveal an increase of the materials hardness with increasing calcium concentration by up to 35 % compared to pure PbTe (Fig. 6). The increased hardness is most probably a result of the more ionic and thus stronger binding of calcium dissolved within the PbTe lattice. Microstructural sources for hardening can be excluded as neither a change of grain size nor precipitations were observed. We believe that CaTe nano precipitates cannot be the reason for the observed hardening: As described above, precipitation of CaTe is assumed to happen mainly in the samples with high calcium concentration, whereas at low concentrations most of the calcium is dissolved in the PbTe matrix. Thus, if precipitation was the reason for the observed hardening, only a small increase would be expected at low calcium concentrations and a steeper increase at high concentrations.

The fracture toughness determined in compression tests increases from 75 to 120 MPa. The observed trend is clear and supported by all samples investigated. Still the absolute values have to be handled with care as sample preparation and invisible cracks within the samples have great influence on the compression test results typically leading to a reduction of the measured values. The compression tests' stress–strain curves (Fig. 6b) qualitatively reveal that the addition of calcium does not lead to increased brittleness despite of increasing hardness and fracture strength. This is in contrast to the effects observed when doping for example with sodium, where the increased fracture strength is accompanied by a strong increase of brittleness [23]. The behaviour of sodium-doped PbTe is associated to the filling of the heavy hole band [23, 25]. As calcium is isoelectronic compared to tellurium, it is assumed to not have a big influence on the filling of the electronic bands and thus does not lead to increased brittleness.

Proof of concept in Na-doped PbTe

As first proof of concept of the calcium approach in doped PbTe as it would be needed for a thermoelectric module, sodium-doped PbTe ($y = 0.014$) with a calcium content of $x = 0.02$ was prepared.

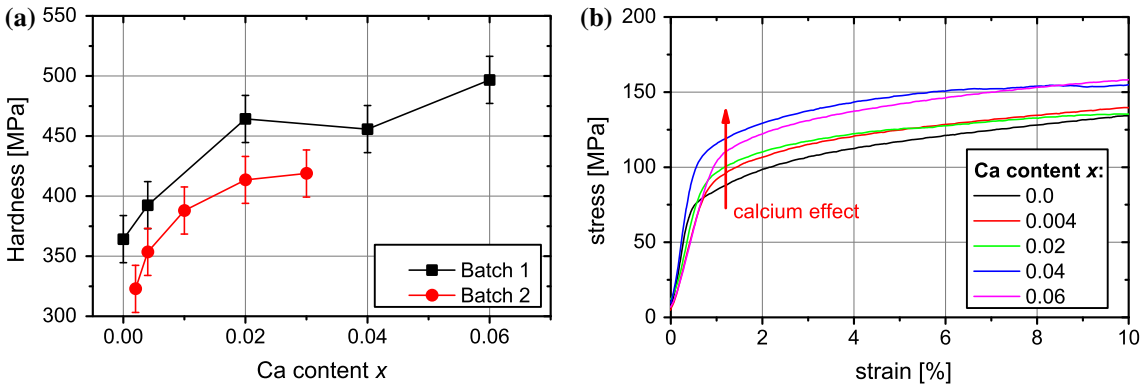

Figure 6 Vickers hardness increases with increasing calcium content (**a**). Stress–strain curves of batch 1 samples determined on cubic samples in uniaxial compression tests showing increased fracture strength due to calcium addition (**b**).

Additionally PbTe samples with varying sodium concentration but without calcium were prepared as reference. All powders and samples prepared appear phase pure in XRD measurements ((Fig. S4 a) in supporting material), fully dense and homogeneous. XRD measurements reveal a decrease of the PbTe lattice constant from 6.460 to 6.457 Å with increasing sodium content in agreement with literature data [48, 51]. A very small reduction of the lattice constant due to additional calcium is indicated but falls within the range of measurement uncertainty ((see Fig. S4b) in supporting material). A stronger reduction of the lattice constant would be expected according to Vegard's law. As discussed earlier this indicates that at least part of the calcium is not dissolved in the matrix but might form precipitates [42].

As expected increasing, the Na concentration increases the electrical conductivity and thus decreases the Seebeck coefficient (Fig. 7). The addition of calcium here slightly reduces the electrical conductivity especially at lower temperatures and increases the Seebeck coefficient, indicating a reduction of free charge carriers and potentially a reduced mobility. A calculation of the charge carrier concentration using Pisarenko's relation would not give valid results in these highly doped samples [48]. Biswas et al. observed increased electrical conductivity and decreased Seebeck coefficients in 1 % Na_2Te-doped samples with ≥3 % CaTe. This is accompanied by an increased carrier concentration and decreased mobility. At lower CaTe concentrations, they observed no influence on the carrier concentration but a slight decrease of the carrier mobility [42]. Their findings are explained as increased dissolution of Na atoms in the PbTe matrix enabled by the addition of calcium. These dissolution effects are not visible in our samples due to the lower Ca and Na concentrations.

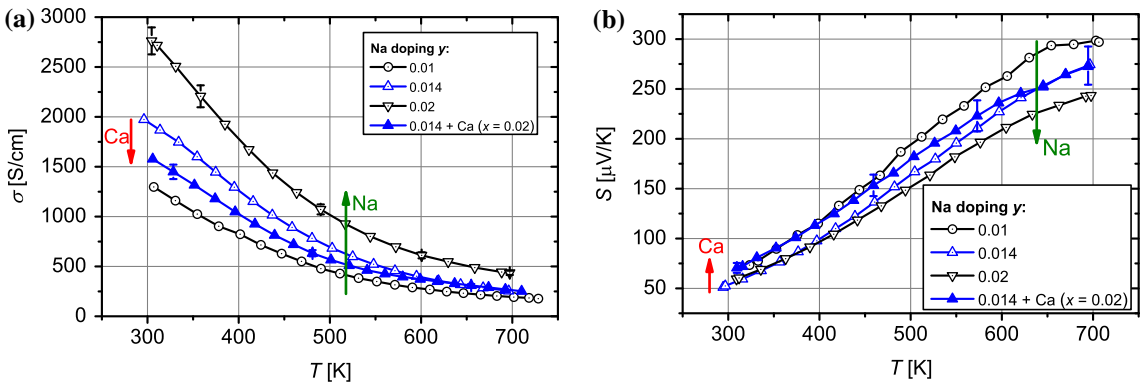

Figure 7 Temperature-dependant electrical conductivity (**a**) and Seebeck coefficient (**b**) of samples doped with sodium and sodium–calcium. Sodium leads to an increase in electrical conductivity and decreasing Seebeck coefficient, whereas the co-doped sample indicates an opposite shift due to calcium.

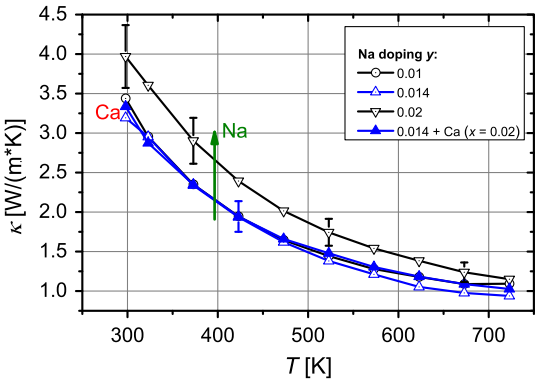

Figure 8 Temperature-dependant thermal conductivity of samples doped with sodium and sodium–calcium. The conductivity increases with increasing sodium content, whereas no effect of calcium addition is observed.

The increase of the thermal conductivity with increasing sodium doping depicted in Fig. 9 can be attributed to an increase of the electronic contribution. The thermal conductivity of the calcium-added sample is expected to be lower than that of the corresponding sample without calcium due to the above-mentioned effects of calcium. Nevertheless measurements illustrated in Fig. 8 show nearly identical thermal conductivities for the samples with $y = 0.01$ and 0.014 as well as the calcium-added sample probably due to measurement uncertainty. This is supported by the observation that at high temperatures the co-doped sample's thermal conductivity appears higher than the purely sodium doped one with equal sodium concentration, which cannot be explained in accordance to all findings described above. It is assumed that the thermal conductivity of the $y = 0.014$ sodium sample is in fact slightly higher than the measured values. Assuming equal lattice thermal conductivity calculations using Wiedemann–Franz law suggest that the thermal conductivity of the $y = 0.014$ sample should be roughly 0.4–0.1 W/(m·K) (at 300 and 700 K, respectively) higher than that of the $y = 0.01$ sample. Still this deviation is within the expected measurement uncertainty of 10 %.

As can be seen in Fig. 9a, b, samples with high power factors and ZT values up to 1.5 at 700 K were achieved, which compare well to literature data [15, 48]. Sample co-doped with calcium has a slightly reduced ZT value mainly due to the reduced electrical conductivity, but still reaches competitively high values exceeding 1.2.

Hardness measurements (Fig. 10a) confirm the already well-known increase of PbTe's hardness with increasing sodium doping [23, 25] and reveal additional hardening due to Calcium. As there is no difference in the microstructure between the Na-/co-doped samples and the samples containing calcium only, it is assumed that again the increased hardness in the co-doped sample is a consequence of the alloying rather than possible formation of nano-scale CaTe precipitates.

Similarly, in compression tests one observes increased fracture toughness and brittleness due to sodium indicated by the drop of the stress–strain curves after reaching the maximum elastic strain (Fig. 10b). In contrast, undoped PbTe is governed by slow crack growth indicated by a smooth stress–strain curve with positive slope in the plastic deformation region (compare Fig. 6b). This change of brittleness is well known for sodium-doped PbTe and attributed to the filling of the heavy hole band [23, 25]. The co-

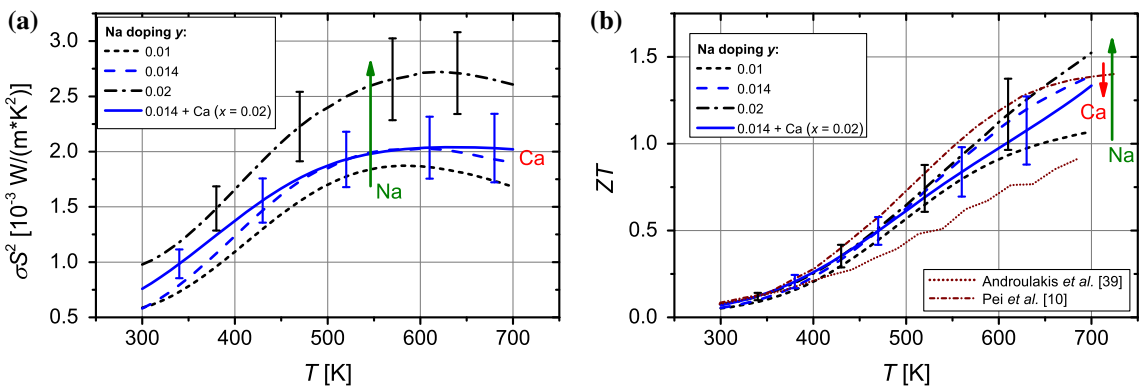

Figure 9 Power factor (**a**) and thermoelectric figure of merit ZT (**b**) of sodium and sodium–calcium doped samples. Calcium addition has only minor influence on both values. Literature data of sodium-doped PbTe is shown for comparison.

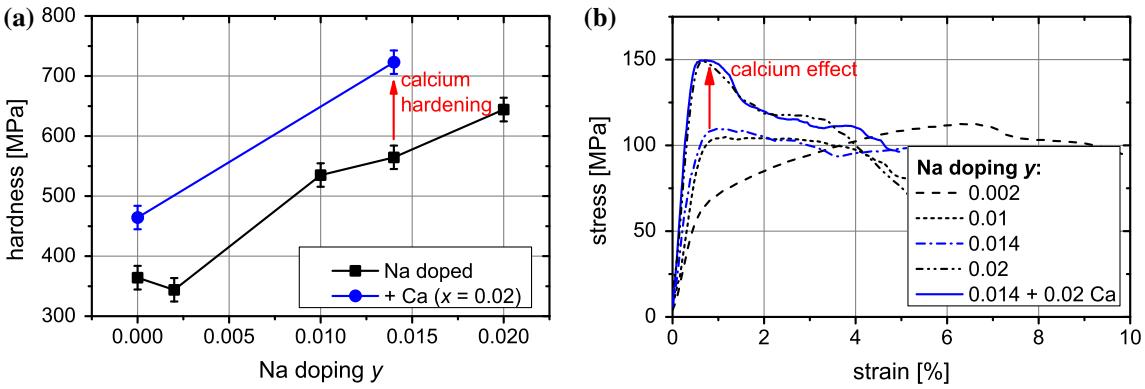

Figure 10 Increasing Vickers hardness with increasing sodium doping and further hardening due to calcium (**a**). Compression tests at room temperature indicate increased fracture toughness in the co-doped sample (**b**).

doped sample indicates an increase in fracture toughness due to calcium, whereas an influence on the brittleness cannot be clearly identified. As mentioned above, changes in Young's modulus or maximum elastic strain cannot be deduced from this data.

Conclusions

Intrinsic and sodium-doped PbTe alloyed with calcium have been prepared. The obtained functional properties in both batches 1 and 2 are very similar although preparation route 2 reduces the content of tellurium-rich phases. An optimized preparation route might improve material properties but an in-depth study of the influence of different parameters during material preparation is beyond the scope of this article and will be published elsewhere.

In intrinsic PbTe, the addition of calcium improves the material's mechanical properties by increasing hardness and fracture strength without increased brittleness. Calcium addition slightly increases the band gap leading to a reduction of the charge carrier concentration and thus electrical conductivity. At higher concentrations, it additionally reduces the carrier mobility and thermal conductivity probably due to the formation of nanoprecipitates. Thus compositions with moderate calcium content as $Pb_{0.98}Ca_{0.02}Te$ seem like a good compromise with significantly improved mechanical properties and only slightly impacted thermoelectric performance. The true solubility of calcium in PbTe and the nature of possible precipitates might be of interest for future in depth studies.

In sodium-doped $Pb_{0.966}Ca_{0.02}Na_{0.014}Te$ material taken as a proof of concept, the negative effects of calcium are much less dominant. The observed reduction in electrical conductivity is nearly fully compensated by an increased Seebeck coefficient and reduced thermal conductivity resulting in a maximum *ZT* above 1.2 around 700 K. The co-doped sample indicates that also in this system calcium increases hardness and fracture strength, whereas no increase in brittleness is observed. Such material properties are most important for production and reliability of TE modules in mass markets and for dynamic operation conditions.

Yet, the co-doped material investigated here is only a first proof of concept and doping levels of co-doped material need to be varied and optimized in a future study. Additionally, the described concept of alloying with electrically non-doping elements to independently tailor mechanical and thermoelectric properties of TE materials might be adapted to other thermoelectric materials and dopants as well.

Acknowledgements

The authors would like to thank the German Federal Ministry of Economics and Technology for funding this research work under Project No. 19U9009C.

Compliance with ethical standards

Conflict of Interest The authors declare that they have no conflict of interest.

Electronic supplementary material: The online version of this article (doi:10.1007/s10853-016-9980-x) contains supplementary material, which is available to authorized users.

References

[1] Crane DT, LaGrandeur JW (2010) Progress report on BSST-led US Department of Energy automotive waste heat recovery program. J Electron Mater 39(9):2142–2148

[2] Bennett GL (1995) Space applications. In: Rowe DM (ed) CRC handbook of thermoelectrics (Chap. 41). CRC, New York

[3] Abelson RD (2005) Space missions and applications. In: Rowe DM (ed) Thermoelectrics handbook—macro to nano (Chap. 56). Taylor & Francis, London

[4] Eder A, Liebl J (2008) Thermoelectric waste heat recovery: a technology transfer from aerospace to the automotive industry? In Jänsch D (ed.), Thermoelektrik: Eine Chance für die Automobilindustrie (Chap. 4). pp 45–56. Expert, Renningen

[5] Case ED (2012) Thermal fatigue and waste heat recovery via thermoelectrics. J Electron Mater 41(6):1811–1819

[6] Xia H, Drymiotis F, Chen C-L, Wu A, Chen Y-Y, Snyder GJ (2015) Bonding and high-temperature reliability of NiFeMo alloy/n-type PbTe joints for thermoelectric module applications. J Mater Sci 50(7):2700–2708. doi:10.1007/s10853-015-8820-8

[7] Schmidt RD, Case ED, Zhao L-D, Kanatzidis MG (2015) Mechanical properties of low-cost, earth-abundant chalcogenide thermoelectric materials, PbSe and PbS, with additions of 0–4% CdS or ZnS. J Mater Sci 50(4):1770–1782. doi:10.1007/s10853-014-8740-z

[8] Ma JM, Firdosy SA, Kaner RB, Fleurial J-P, Ravi VA (2014) Hardness and fracture toughness of thermoelectric $La_{3-x}Te_4$. J Mater Sci 49(3):1150–1156. doi:10.1007/s10853-013-7794-7

[9] Schmidt RD, Fan X, Case ED, Sarac PB (2015) Mechanical properties of Mg_2Si thermoelectric materials with the addition of 0–4 vol% silicon carbide nanoparticles (SiCNP). J Mater Sci 50(11):4034–4046. doi:10.1007/s10853-015-8960-x

[10] Schmidt RD, Case ED, Lobo Z, Thompson TR, Sakamoto JS, Zhou X-Y, Uher C (2014) Influence of silver nanoparticle addition, porosity, and processing technique on the mechanical properties of $Ba_{0.3}Co_4Sb_{12}$ skutterudites. J Mater Sci 49(20):7192–7212. doi:10.1007/s10853-014-8427-5

[11] Ravich YI, Efimova BA, Smirnov IA (1970) Semiconducting lead chalcogenides. Plenum, New York

[12] Dughaish ZH (2002) Lead telluride as a thermoelectric material for thermoelectric power generation. Physica B 322:205–223

[13] Biswas K, He J, Blum ID, Wu C-I, Hogan TP, Seidman DN, Dravid VP, Kanatzidis MG (2012) High-performance bulk thermoelectrics with all-scale hierarchical architectures. Nature 489:414–418

[14] LaLonde AD, Pei Y, Snyder GJ (2011) Reevaluation of $PbTe_{1-x}Ix$ as high performance n-type thermoelectric material. Energy Environ Sci 4:2090–2096

[15] Pei Y, LaLonde A, Iwanaga S, Snyder GJ (2011) High thermoelectric figure of merit in heavy hole dominated PbTe. Energy Environ Sci 4:2085–2089

[16] Pei Y, Shi X, LaLonde A, Wang H, Chen L, Snyder GJ (2011) Convergence of electronic bands for high performance bulk thermoelectrics. Nature 473:66–69

[17] Long C, Hou X, Gelbstein Y, Zhang J, Ren B, Wang Z (2006) Preparation and thermoelectric properties of n-type *PbTe* doped with *In* and PbI_2. In Proceedings: 25th international conference on thermoelectrics (ICT), pp 382–385

[18] Gelbstein Y, Davidow J, Girard SN, Chung DY, Kanatzidis M (2013) Controlling metallurgical phase separation reactions of the $Ge_{0.87}Pb_{0.13}Te$ alloy for high thermoelectric performance. Adv Energy Mater 3:815–820

[19] Wu D, Zhao L-D, Wu QH, Chi H, Gelbstein Y, Uher C, Wolverton C, Kanatzidis M, He J (2014) Origin of the high performance in GeTe-based thermoelectric materials. J Am Chem Soc 136:11412–11419

[20] Madelung O, Rössler U, Schulz M (eds) (1998) Landolt-Börnstein: Group III condensed matter non-tetrahedrally bonded elements and binary compounds I, vol 41c. Springer, Berlin

[21] Houston B, Strakna RE, Belson HS (1968) Elastic constants, thermal expansion, and Debye temperature of lead telluride. J Appl Phys 39(8):3913–3916

[22] Einspruch NG, Manning RJ (1963) Elastic constants of compound semiconductors—*ZnS*, *PbTe*. GaSb J Acoust Soc Am 35(2):215–216

[23] Ablova MS (1971) Effect of donor and acceptor additions on the mechanical properties of *PbTe*, *PbSe* and *PbS*. Sov. Phys. Sol. State 12(12):2910–2912

[24] Tsypin MI, Chipzhenko AA, Kulikova GA, Ostrovskaya LM, Dubrovina AN, Kvyatkovskii LE (1973) Mechanical properties of certain semiconductors. Inorg. Mater. (USSR) 9(7):1112–1113

[25] Gelbstein Y, Gotesman G, Lishzinker Y, Dashevsky Z, Dariel MP (2008) Mechanical properties of *PbTe*-based thermoelectric semiconductors. Scr Mater 58:251–254

[26] Ren F, Case ED, Sootsman JR, Kanatzidis MG, Kong H, Uher C, Lara-Curzio E, Trejo RM (2008) The high-temperature elastic moduli of polycrystalline *PbTe* measured by resonant ultrasound spectroscopy. Acta Mater 56:5954–5963

[27] Zlatanov ZK (2007) Mechanical properties and structure of *Gd*-doped *PbTe*. Mater Chem Phys 103:470–474

[28] Davidow J, Gelbstein Y (2013) A comparison between the mechanical and thermoelectric properties of the highly efficient p-type GeTe rich compositions—TAGS-80, TAGS-85 and 3% Bi_2Te_3 doped $Ge_{0.87}Pb_{0.13}Te$. J Electron Mater 42(7):1542–1549

[29] Eiss AL (1966) Studies of lead telluride thermoelectric elements. In *Proceedings: thermoelectric specialists conference, IEEE/AIAA*, pp 20451–204519

[30] Darrow MS, White WB, Roy R (1969) Micro-indentation hardness variation as a function of composition for polycrystalline solutions in the systems *PbS/PbTe*, *PbSe/PbTe*, and *PbS/PbSe*. J Mater Sci 4:313–319. doi:10.1007/BF00550400

[31] Sootsman JR, He J, Dravid VP, Ballikaya S, Vermeulen D, Uher C, Kanatzidis MG (2010) Microstructure and thermoelectric properties of mechanically robust *PbTe-Si* eutectic composites. Chem Mater 22:869–875

[32] Gorelik SS, Dubrovina AN, Kvyatkovskii LE, Ostrovskaya LM, Chipzhenko AA, Tsypin MI (1973) The deformation mechanism in certain thermoelectric materials. Russ Phys J 16(12):1655–1658

[33] Sifi C, Meradji H, Slimani M, Labidi S, Ghemid S, Hanneche EB, El Haj Hassan F (2009) First principle calculations of structural, electronic, thermodynamic and optical properties of $Pb_{1-x}Ca_xS$, $Pb_{1-x}Ca_xSe$ and $Pb_{1-x}Ca_xTe$ ternary alloys. J Phys Condens Matter 21:195401

[34] Ahn K, Li C, Uher C, Kanatzidis MG (2009) Improvement in the thermoelectric figure of merit by *La*/*Ag* cosubstitution in *PbTe*. Chem Mater 21:1361–1367

[35] O'Connor BH, Li DY, Hunter BA (2001) The importance of the specimen displacement correction in Rietveld pattern fitting with symmetric reflection-optics diffraction data. Adv X-Ray Anal 44:96–102

[36] O'Connor BH, Pratapa S (2002) Improving the accuracy of Rietveld-derived lattice parameters by an order of magnitude. Adv X-Ray Anal 45:158–165

[37] Platzek D, Karpinski G, Drasar C, Müller E (2005) Seebeck scanning microprobe for thermoelectric FGM. Mater Sci Forum 492–493:587–592

[38] Matsushita Y, Wianecki PA, Sommer AT, Geballe TH, Fisher IR (2006) Type ii superconducting parameters of *Tl*-doped *PbTe* determined from heat capacity and electronic transport measurements. Phys Rev B 74(13):134512

[39] Wohlrab M (1966) Die spezifische wärme von Bi_2Te_3, *CdTe,* PbTe und SnTe. Ann Phys 472:89–90

[40] de Boor J, Stiewe C, Ziolkowski P, Dasgupta T, Karpinski G, Lenz E, Edler F, Müller E (2013) High temperature measurement of Seebeck coefficient and electrical conductivity. J Electron Mater 42:1711–1718

[41] de Boor J, Müller E (2013) Data analysis for Seebeck coefficient measurements. Rev Sci Instrum 84:065102

[42] Biswas K, He J, Wang G, Lo S-H, Uher C, Dravid VP, Kanatzidis MG (2011) High thermoelectric figure of merit in nanostructured p-type PbTe-MTe (M = Ca, Ba). Energy Environ Sci 4:4675–4684

[43] Brebrick RF, Allgaier RS (1960) Composition limits of stability of *PbTe*. J Chem Phys 32(6):1826–1831

[44] Heikes RR, Ure RW (1961) Thermoelectricity: science and engineering. Interscience, New York

[45] Ahmad S, Mahanti SD, Hoang K, Kanatzidis MG (2006) Ab initio studies of electronic structure of defects in *PbTe*. Phys Rev B 74(15):1–13

[46] Appel J (1961) Remark on the Seebeck coefficient of polar semiconductors. Philos Mag 6:167–169

[47] Ioffe AF (1958) Physik der Halbleiter. Akademie, Berlin

[48] Androulakis J, Todorov I, Chung D-Y, Ballikaya S, Wang G, Uher C, Kanatzidis MG (2010) Thermoelectric enhancement in *PbTe* with *K* or *Na* codoping from tuning the interaction of the light- and heavy-hole valence bands. Phys Rev B 82:115209

[49] Yoneda S, Ohta E, Kaibe HT, Shiota I, Takahashi K, Shinohara Y, Imai Y, Nishida IA (1997) Crystal grain size dependence of thermoelectric properties for sintered *PbTe* by spark plasma sintering technique. In: Proceedings: 16th international conference on thermoelectrics (ICT), pp 247–250

[50] Partin DL, Clemens BM, Swets DE, Thrush CM (1986) Lead calcium telluride grown by molecular beam epitaxy. J Vac Sci Technol B 4(2):578–580

[51] Biswas K, He J, Zhang Q, Wang G, Uher C, Dravid VP, Kanatzidis MG (2011) Strained endotaxial nanostructures with high thermoelectric figure of merit. Nat Chem 3:160–166